

## Mechanistic Pathways for N<sub>2</sub>O Elimination from *trans*-R<sub>3</sub>Sn-O-N=N-O-SnR<sub>3</sub> and for Reversible Binding of CO<sub>2</sub> to R<sub>3</sub>Sn-O-SnR<sub>3</sub> (R = Ph, Cy)

Jack V. Davis,<sup>§</sup> Mohan M. Gamage,<sup>§</sup> Oswaldo Guio, Burjor Captain,<sup>\*</sup> Manuel Temprado,<sup>\*</sup> and Carl D. Hoff<sup>\*</sup>

Cite This: <https://doi.org/10.1021/acs.inorgchem.1c01291>

Read Online

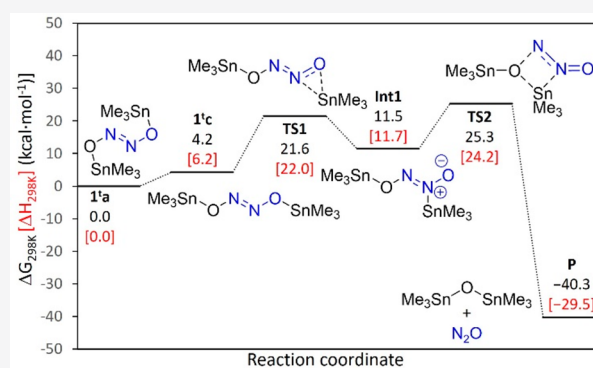
ACCESS |

Metrics & More

Article Recommendations

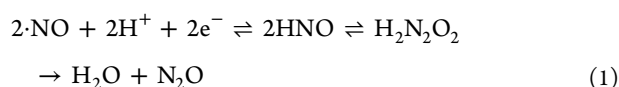
Supporting Information

**ABSTRACT:** The rate and mechanism of the elimination of N<sub>2</sub>O from *trans*-R<sub>3</sub>Sn-O-N=N-O-SnR<sub>3</sub> (R = Ph (**1<sup>Ph</sup>**) and R = Cy (**1<sup>Cy</sup>**)) to form R<sub>3</sub>Sn-O-SnR<sub>3</sub> (R = Ph (**2<sup>Ph</sup>**) and R = Cy (**2<sup>Cy</sup>**)) have been studied using both NMR and IR techniques to monitor the reactions in the temperature range of 39–79 °C in C<sub>6</sub>D<sub>6</sub>. Activation parameters for this reaction are  $\Delta H^\ddagger = 15.8 \pm 2.0$  kcal·mol<sup>-1</sup> and  $\Delta S^\ddagger = -28.5 \pm 5$  cal·mol<sup>-1</sup>·K<sup>-1</sup> for **1<sup>Ph</sup>** and  $\Delta H^\ddagger = 22.7 \pm 2.5$  kcal·mol<sup>-1</sup> and  $\Delta S^\ddagger = -12.4 \pm 6$  cal·mol<sup>-1</sup>·K<sup>-1</sup> for **1<sup>Cy</sup>**. Addition of O<sub>2</sub>, CO<sub>2</sub>, N<sub>2</sub>O, or PPh<sub>3</sub> to sealed tube NMR experiments did not alter in a detectable way the rate or product distribution of the reactions. Computational DFT studies of elimination of hyponitrite from *trans*-Me<sub>3</sub>Sn-O-N=N-O-SnMe<sub>3</sub> (**1<sup>Me</sup>**) yield a mechanism involving initial migration of the R<sub>3</sub>Sn group from O to N passing through a marginally stable intermediate product and subsequent N<sub>2</sub>O elimination. Reactions of **1<sup>Ph</sup>** with protic acids HX are rapid and lead to formation of R<sub>3</sub>SnX and *trans*-H<sub>2</sub>N<sub>2</sub>O<sub>2</sub>. Reaction of **1<sup>Ph</sup>** with the metal radical •Cr(CO)<sub>3</sub>C<sub>3</sub>Me<sub>5</sub> at low concentrations results in rapid evolution of N<sub>2</sub>O. At higher •Cr(CO)<sub>3</sub>C<sub>3</sub>Me<sub>5</sub> concentrations, evolution of CO<sub>2</sub> rather than N<sub>2</sub>O is observed. Addition of 1 atm or less CO<sub>2</sub> to benzene or toluene solutions of **2<sup>Ph</sup>** and **2<sup>Cy</sup>** resulted in very rapid reaction to form the corresponding carbonates R<sub>3</sub>Sn-O-C(=O)-O-SnR<sub>3</sub> (R = Ph (**3<sup>Ph</sup>**) and R = Cy (**3<sup>Cy</sup>**)) at room temperature. Evacuation results in fast loss of bound CO<sub>2</sub> and regeneration of **2<sup>Ph</sup>** and **2<sup>Cy</sup>**. Variable temperature data for formation of **3<sup>Cy</sup>** yield  $\Delta H^\circ = -8.7 \pm 0.6$  kcal·mol<sup>-1</sup>,  $\Delta S^\circ = -17.1 \pm 2.0$  cal·mol<sup>-1</sup>·K<sup>-1</sup>, and  $\Delta G^\circ_{298K} = -3.6 \pm 1.2$  kcal·mol<sup>-1</sup>. DFT studies were performed and provide additional insight into the energetics and mechanisms for the reactions.

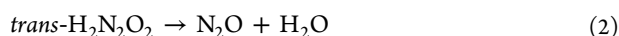


### INTRODUCTION

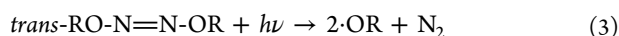
Hyponitrites are an important class of intermediates involved in the metal mediated two electron reduction of nitric oxide to nitrous oxide by nitric oxide reductases<sup>1</sup> as shown in [reaction 1](#).



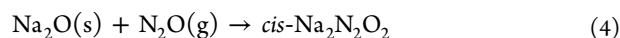
The rate of N<sub>2</sub>O elimination, the last step of [eq 1](#), has been extensively studied for the more stable *trans* isomer as shown in [reaction 2](#) and depends on a number of factors including pH, the presence of radicals, and electrophiles.<sup>2</sup>



Likewise, the reactions of organic esters of hyponitrite have been extensively studied photochemically<sup>3</sup> where they are a source of organic radicals ([reaction 3](#)).



While nitrous oxide elimination from hyponitrites is common, examples of N<sub>2</sub>O addition to metal oxides to form hyponitrite complexes are rare. In this regard, Feldmann and Jansen<sup>4</sup> reported formation of pure crystalline *cis*-Na<sub>2</sub>N<sub>2</sub>O<sub>2</sub> at 360 °C as shown in [reaction 4](#).



We have recently reported *in situ* preparation of *cis*-Na<sub>2</sub>N<sub>2</sub>O<sub>2</sub> by mechanochemical methods and its further oxidation to nitrate in a mixer mill under 2 atm pressure of nitrous oxide at much lower temperatures of 38 °C.<sup>5</sup> While the examples of N<sub>2</sub>O addition to complexes forming hyponitrites are limited,

Received: April 27, 2021

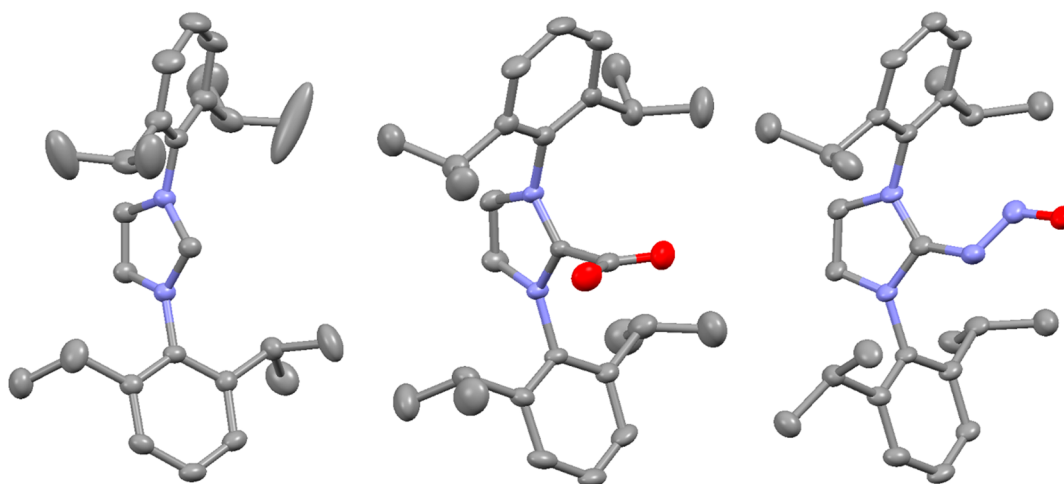


**Figure 1.** Structures (40% thermal ellipsoids) of the IPr (left),<sup>9</sup> IPr-CO<sub>2</sub> (center),<sup>7</sup> and IPr-N<sub>2</sub>O (right)<sup>8</sup> highlighting the differing architectures for the adducts [carbon (gray), nitrogen (light blue), oxygen (red)], (IPr = 1,3-bis(diisopropyl)phenylimidazol-2-ylidene).

the analogous reactions with isoelectronic CO<sub>2</sub> leading to carbonates are more common and have been much more explored.<sup>6</sup> The fact that a much larger number of carbonate complexes exist compared to hyponitrite complexes implies greater kinetic access and also more thermodynamic stability for carbonates. The structures of N-heterocyclic carbene (NHC) adducts of CO<sub>2</sub><sup>7</sup> and N<sub>2</sub>O<sup>8</sup> are both known, and they are shown in Figure 1. These Lewis acid-Lewis base pairs may serve as models for possible initial binding in the formation of the corresponding hyponitrites or carbonates.

Somewhat surprisingly, available data show similar approximate enthalpies of binding and stability<sup>10</sup> for the different binding motifs displayed by the NHC adducts of N<sub>2</sub>O and CO<sub>2</sub>. In addition, Roesler and co-workers have recently isolated and structurally characterized  $\eta^2$  complexes of both CO<sub>2</sub> and N<sub>2</sub>O to a (NHC)<sub>2</sub>Ni<sup>0</sup> fragment with similar computed enthalpies of binding.<sup>11</sup>

Information regarding the mechanism and energetics of hyponitrite formation may be obtained by study of the mechanism of nitrous oxide elimination using the principle of microscopic reversibility. The work reported here compares irreversible elimination of nitrous oxide from *trans*-[(R<sub>3</sub>Sn)<sub>2</sub>( $\mu$ -N<sub>2</sub>O<sub>2</sub>)] (R = phenyl and cyclohexyl) hyponitrite complexes to reversible carbon dioxide capture of R<sub>3</sub>Sn-O-SnR<sub>3</sub> compounds as shown in Scheme 1.

## EXPERIMENTAL SECTION

Please see the Supporting Information (SI) for experimental details and procedures.

## RESULTS

**Synthesis and Crystal Structure of *trans*-[(Cy<sub>3</sub>Sn)<sub>2</sub>( $\mu$ -N<sub>2</sub>O<sub>2</sub>)]**, **1<sup>Cy</sup>**. The reaction of 2 equivalents of Cy<sub>3</sub>SnCl with *trans*-Ag<sub>2</sub>N<sub>2</sub>O<sub>2</sub> resulted in the formation of *trans*-[(Cy<sub>3</sub>Sn)<sub>2</sub>( $\mu$ -N<sub>2</sub>O<sub>2</sub>)]<sub>2</sub>, **1<sup>Cy</sup>**, and AgCl. Slow evaporation of the reaction mixture after the removal of AgCl resulted in the formation of colorless crystals in 70.9% yield. The complex was characterized by a combination of <sup>119</sup>Sn NMR and single crystal X-ray diffraction analyses. An ORTEP showing the molecular structure of compound **1<sup>Cy</sup>** is shown in Figure 2. Selected structural data are listed in Table 1.

Analysis of crystal structures for **1<sup>Cy</sup>** and that of previously reported<sup>12,13</sup> for **1<sup>Ph</sup>** revealed that both compounds have very

## Scheme 1. Binding and Dissociation Reactions Studied in This Work

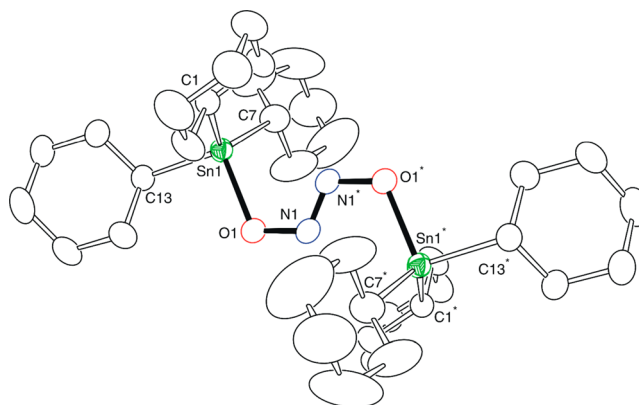
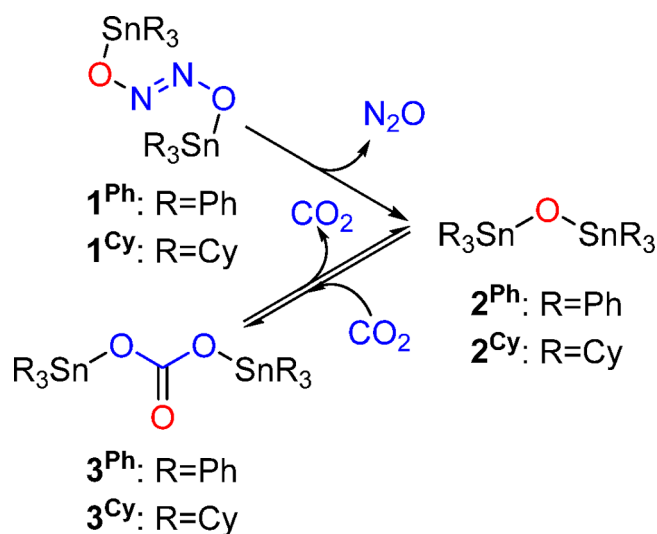


**Figure 2.** An ORTEP of the molecular structure of **1<sup>Cy</sup>** showing 40% probability thermal ellipsoids. Complete crystallographic data and files are available in the SI.

similar bond distances and angles. Measurement of Sn–N distances showed that the Sn(1)–N(1\*) distances are shorter than the Sn(1)–N(1) distances for both compounds. These

**Table 1.** Selected Intramolecular Distances and Angles for  $1^{Cy}$ <sup>a</sup>

atoms	distance (Å)	atoms	angle (deg)
N(1)–N(1*)	1.226(7)	N(1*)–N(1)–O(1)	112.2(4)
N(1)–O(1)	1.367(4)	N(1)–O(1)–Sn(1)	114.0(2)
O(1)–Sn(1)	2.073(3)	O(1)–Sn(1)–C(1)	107.56(14)
Sn(1)–N(1)	2.912	O(1)–Sn(1)–C(7)	105.99(17)
Sn(1)–N(1*)	2.782	O(1)–Sn(1)–C(13)	96.70(13)
Sn(1)–C(1)	2.169(4)	Sn(1)–C(1)–C(2)	114.8(3)
Sn(1)–C(7)	2.173(4)	Sn(1)–C(1)–C(6)	110.0(3)
Sn(1)–C(13)	2.157(4)		
C(1)–C(2)	1.513(5)		

<sup>a</sup>Estimated standard deviations (ESD) in the least significant figure are given in parentheses.

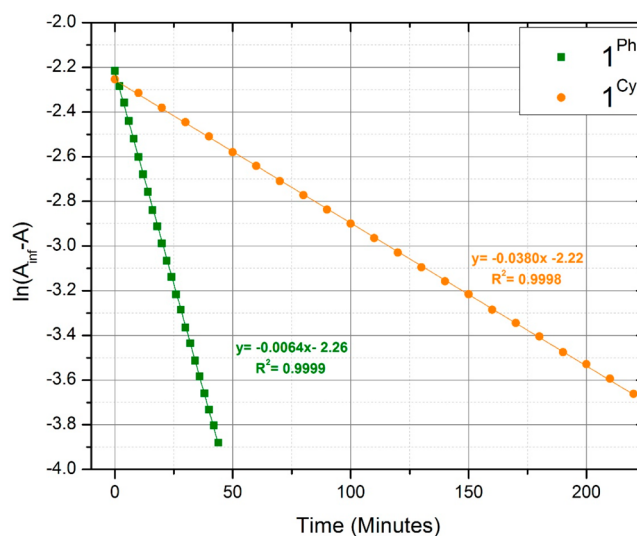
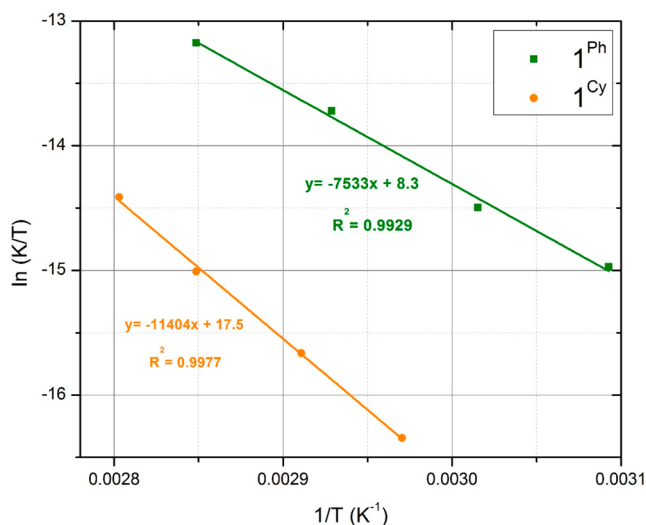
Sn–N distances are long for bonding interactions as Sn can certainly be 5-coordinate. However, it has been reported that the Sn–N bond distances for 5-coordinate Sn complexes obtained by the reactions of triorganotin chlorides with 2-mercaptopyrimidines<sup>14</sup> are in the range of Sn–N distances obtained for *trans*-bisstanny hyponitrites and may imply some Sn–N bonding interactions for 5-coordinate Sn.<sup>15</sup>

Comparison of crystal structures of  $1^{Cy}$  and  $1^{Ph}$  with that of  $[(OEP)Fe]_2(\mu-N_2O_2)$  showed a significant difference in the metal atom position. Sn atoms in  $1^{Cy}$  and  $1^{Ph}$  are bent toward the N=N bond so that both the Sn atoms are positioned beside the N=N bond, whereas the Fe atoms in  $[(OEP)Fe]_2(\mu-N_2O_2)$ <sup>16</sup> are positioned away from the N=N bond which could be due to the geometry of the OEP ligand.

**NMR Studies of Thermal Decomposition of  $1^{Ph}$  and  $1^{Cy}$ .** Thermal treatment of solutions of *trans*- $[(R_3Sn)_2(\mu-N_2O_2)]$  species leads to slow elimination of  $N_2O$  and the formation of the corresponding distannoxanes. The attempts to study the thermal decomposition of  $1^{Ph}$  and  $1^{Cy}$  by variable temperature  $^{119}Sn$  NMR were unsuccessful due to the broadening of peaks assigned to  $1^{Ph}$  and  $1^{Cy}$  at higher temperatures. Therefore, NMR samples were heated in a temperature-controlled water bath for a certain time, and then the samples were removed and allowed to equilibrate at room temperature before  $^{119}Sn$  NMR spectra were taken. The rate of decomposition of  $1^{Ph}$  was determined by the ratio of the integrated peak area for  $1^{Ph}$  to the total integrated peak areas for tin. The thermal decomposition rate for compound  $1^{Ph}$  at 70 °C observed by  $^{119}Sn$  NMR is shown in the SI. The attempts to study the thermal decomposition of  $1^{Cy}$  by  $^{119}Sn$  NMR were unsuccessful even at room temperature due to the peak broadening caused by rapid ring flipping of cyclohexyl rings.

**FTIR Studies of Thermal Decomposition of  $1^{Ph}$  and  $1^{Cy}$ .** FTIR provided a more efficient and accurate method to determine the rates of thermal decomposition for  $1^{Ph}$  and  $1^{Cy}$  by measuring the absorbance of the FTIR band assigned to nitrous oxide at 2219  $cm^{-1}$  in benzene solutions. Representative data for the thermal decomposition rates for these compounds at 77.9 °C observed by FTIR are shown in Figure 3.

Eyring plots for the thermal decomposition of compounds  $1^{Ph}$  and  $1^{Cy}$  are shown in Figure 4. Analysis of the Eyring plots allowed determination of the experimental activation parameters shown in Table 2 for the thermal decomposition of compounds  $1^{Ph}$  and  $1^{Cy}$  to produce the corresponding distannoxane with the elimination of nitrous oxide as shown

**Figure 3.** Comparison of the first order reaction profiles for thermal decomposition of compounds  $1^{Ph}$  and  $1^{Cy}$  at 77.9 °C.**Figure 4.** Eyring plots ( $\ln[k/T]$  vs  $1/T$ ) for thermal decomposition of compounds  $1^{Ph}$  and  $1^{Cy}$ .**Table 2.** Experimental Activation Parameters Obtained for Thermal Decomposition of Compounds  $1^{Ph}$  and  $1^{Cy}$ 

	$1^{Cy}$	$1^{Ph}$
$\Delta H^\ddagger$ (kcal·mol <sup>-1</sup> )	22.7 ± 2.5	15.8 ± 2.0
$\Delta S^\ddagger$ (cal·mol <sup>-1</sup> ·K <sup>-1</sup> )	-12.5 ± 6	-28.5 ± 5

in Scheme 1. Results indicate that the compound  $1^{Cy}$  has an enthalpy of activation, approximately 7 kcal·mol<sup>-1</sup> higher than that of the compound  $1^{Ph}$  but a less unfavorable entropy of activation.

**Reaction of  $1^{Ph}$  with  $\bullet Cr(CO)_3C_5Me_5$  (Low Radical Loading).** Reactions of  $1^{Ph}$  with  $\bullet Cr(CO)_3C_5Me_5$  using a low loading (15% mol) of  $\bullet Cr(CO)_3C_5Me_5$  relative to compound  $1^{Ph}$  at room temperature resulted in near complete loss of  $N_2O$  in less than an hour, compared to several days for an uncatalyzed reaction. A plausible mechanistic scheme consistent with our experimental observations and calculations (*vide infra*) is shown in Scheme 2.

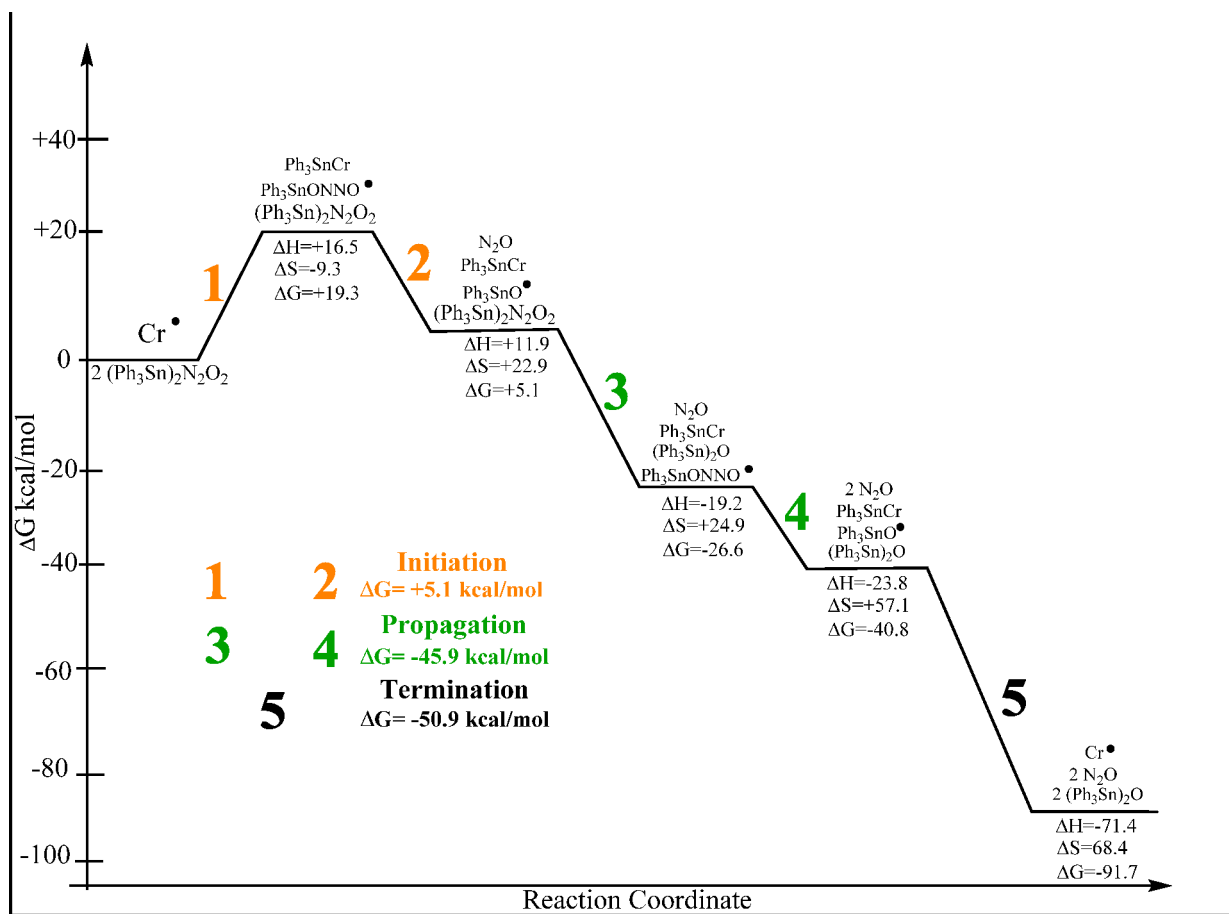
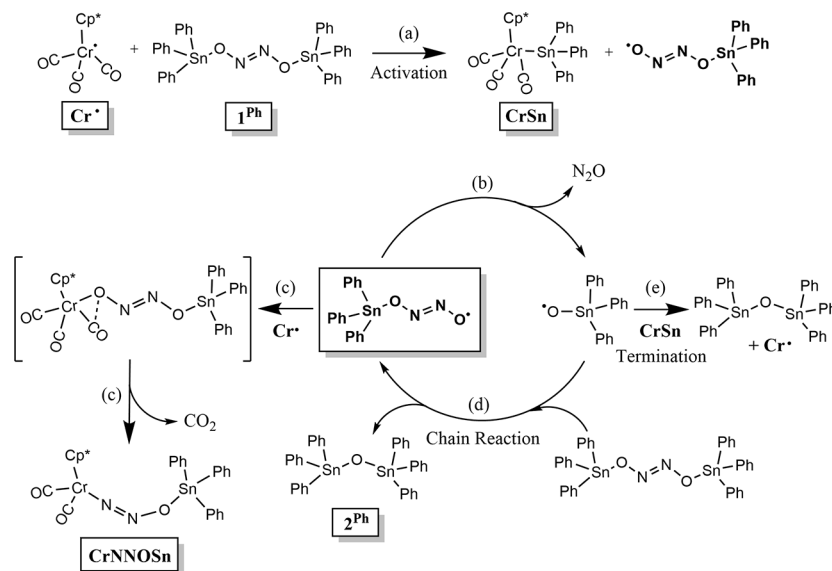
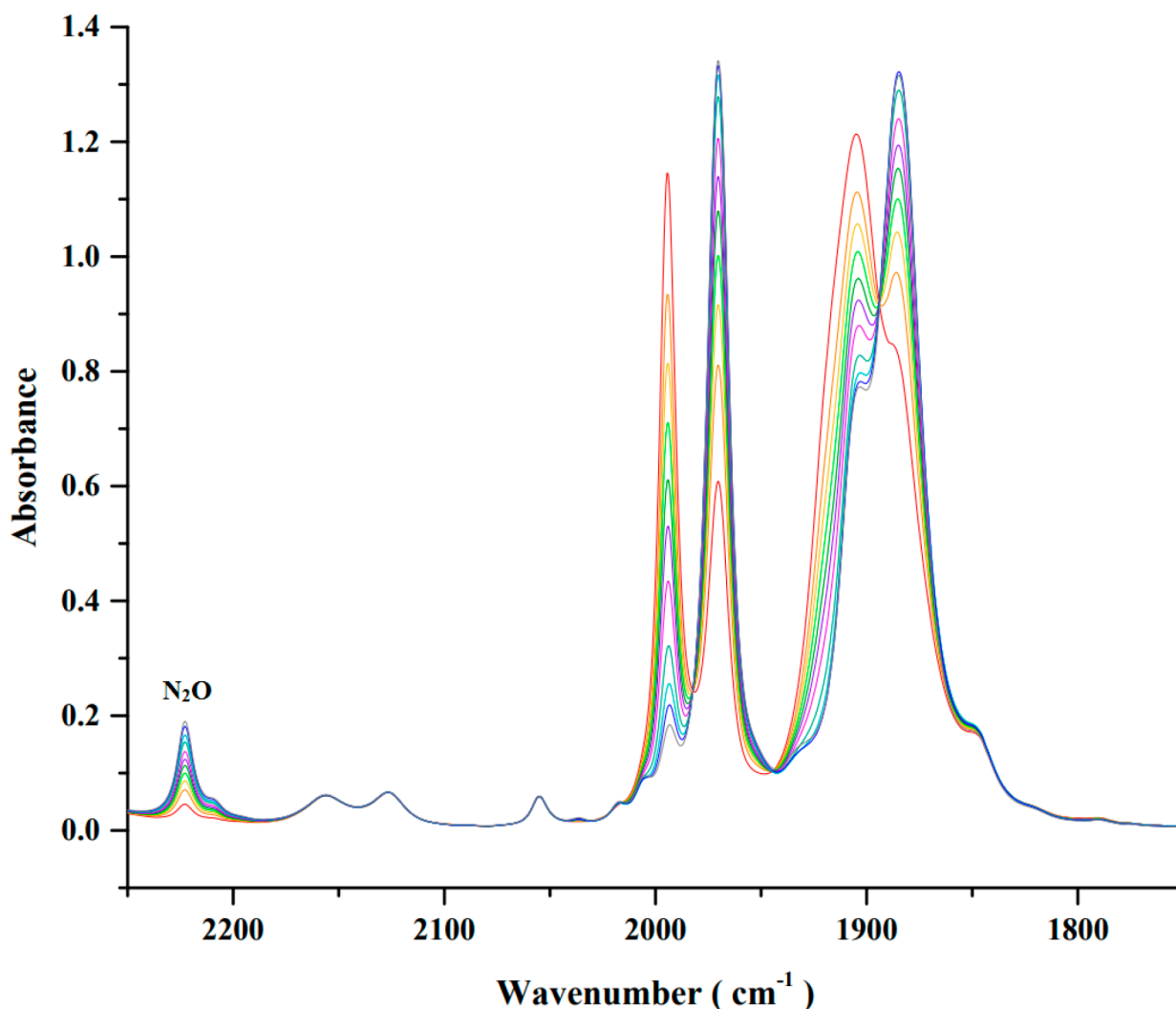
Scheme 2. Proposed Mechanism for N<sub>2</sub>O Elimination from 1<sup>Ph</sup> Promoted by •Cr(CO)<sub>3</sub>Cp\* (Cp\* = C<sub>5</sub>Me<sub>5</sub>).

Figure 5. Computed thermodynamic profile (kcal·mol<sup>-1</sup>) for stoichiometric reduction of 2 mol of 1<sup>Ph</sup> promoted by •Cr(CO)<sub>3</sub>C<sub>5</sub>Me<sub>5</sub>. Steps 1 and 2 serve to generate a •OSnPh<sub>3</sub> radical which may participate in a chain reaction, steps 3 and 4, and end in termination step 5.

Step (a) in Scheme 2 shows the uphill production of the •ON=N-O-SnPh<sub>3</sub> radical and the known Ph<sub>3</sub>Sn-Cr(CO)<sub>3</sub>C<sub>5</sub>Me<sub>5</sub> compound.<sup>17</sup> The oxygen centered radical produced in this way may either combine with a second equivalent of •Cr(CO)<sub>3</sub>C<sub>5</sub>Me<sub>5</sub> in step (c) or lose N<sub>2</sub>O to generate •OSnPh<sub>3</sub> in step (b) and enter into the radical chain

reaction shown in step (d). Several termination steps are possible such as that shown in reaction (e). The enhanced rate of loss of N<sub>2</sub>O from 1<sup>Ph</sup> promoted by the presence of •Cr(CO)<sub>3</sub>C<sub>5</sub>Me<sub>5</sub> is not reproducible and not predictable. The same behavior has been observed in other hyponitrite reactions<sup>2</sup> and is often associated with radical processes



**Figure 6.** FTIR spectra obtained for the reaction of compound  $1^{\text{Ph}}$  with 2.5 equivalents of  $\text{HCr}(\text{CO})_3\text{C}_5\text{Me}_5$  in methylene chloride at room temperature. The steady growth of  $\text{N}_2\text{O}$  is shown at  $2219\text{ cm}^{-1}$ . Data showing the growth and decay of the band assigned to *trans*- $\text{H}_2\text{N}_2\text{O}_2$  as well as the growth of a band assigned to  $\text{H}_2\text{O}$  are available in the SI.

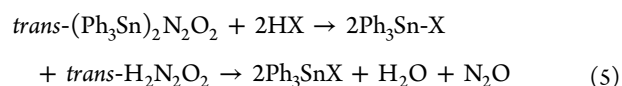
where chain termination steps may occur with a number of reagents.

DFT calculations at the B3LYP-D3(BJ)/Def2-TZVP//B3LYP-D3(BJ)/Def2-SVP level of theory<sup>20–22</sup> in the gas phase were performed to analyze the thermodynamics of this transformation, and the computed data obtained are schematically shown in Figure 5, supporting the viability of the mechanism proposed in Scheme 2.

**Reaction of  $1^{\text{Ph}}$  with  $\bullet\text{Cr}(\text{CO})_3\text{C}_5\text{Me}_5$  (High Radical Loading).** Addition of 400 equivalents of  $\bullet\text{Cr}(\text{CO})_3\text{C}_5\text{Me}_5$  to compound  $1^{\text{Ph}}$  at room temperature resulted in the formation of 10 times more carbon dioxide than nitrous oxide. In parallel with  $\text{CO}_2$  evolution, solution FTIR data showed the formation of a complex which slowly decomposes in solution and is formulated as “ $\text{Cr}(\text{C}_5\text{Me}_5)(\text{CO})_2(\text{NNO-SnPh}_3)$ ” based on its experimental and computed IR spectrum as discussed in the SI. This complex resembles the highly stable nitrosyl complex  $\text{Cr}(\text{C}_5\text{Me}_5)(\text{CO})_2(\text{NO})$ ,<sup>17</sup> and its formation is proposed to occur by step (c) in Scheme 2. Attempts to isolate and crystallographically characterize the proposed  $\text{Cr}(\text{C}_5\text{Me}_5)(\text{CO})_2(\text{NNO-SnPh}_3)$  complex have so far been unsuccessful.

**Reaction of  $1^{\text{Ph}}$  with Protic Acids, HAc, HSPH, and  $\text{HCr}(\text{CO})_3(\text{C}_5\text{Me}_5)$ .** Reaction of  $1^{\text{Ph}}$  with protic acids in

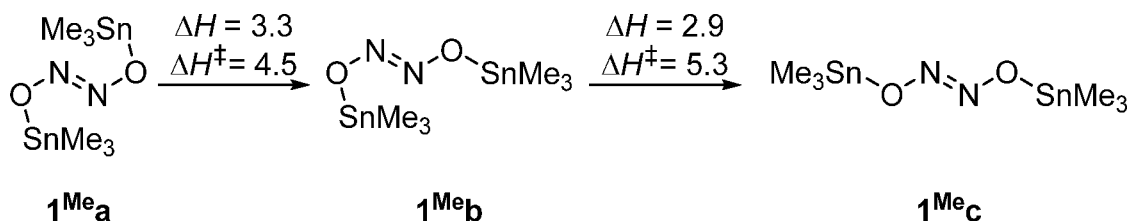
benzene or methylene chloride was found to occur rapidly as shown in eq 5 for  $\text{X} = \text{OAc}$ , SPh,  $\text{Cr}(\text{CO})_3\text{C}_5\text{Me}_5$ .



FTIR data for the reaction of  $1^{\text{Ph}}$  with 2.5 equivalents of the weak acid  $\text{HCr}(\text{CO})_3(\text{C}_5\text{Me}_5)$  in methylene chloride at room temperature are shown in Figure 6.

The overall reaction is rapid with over 90% of  $1^{\text{Ph}}$  consumed within 10 min of mixing the reagents. The decomposition of hyponitrous acid to  $\text{N}_2\text{O}$  and  $\text{H}_2\text{O}$  occurs at a slightly slower rate. The rates of the reaction and its products are qualitatively similar for the chromium hydride and for example acetic acid. However, it should be noted that, due to the weak nature of the Cr–H bond,<sup>17</sup> more complex H atom transfer reactions cannot be ruled out.

**Effect of the Addition of  $\text{O}_2$ ,  $\text{CO}_2$ ,  $\text{N}_2\text{O}$ , or  $\text{PPh}_3$  on Decomposition of  $1^{\text{Ph}}$ .** Little change in the rate of conversion of  $1^{\text{Ph}}$  to stannoxane and nitrous oxide was observed when the reaction was performed under an atmosphere of  $\text{O}_2$ ,  $\text{CO}_2$ , or  $\text{N}_2\text{O}$  rather than argon. Addition

Scheme 3. Isomerization Reactions for the  $1^{\text{Me}}$  Hyponitrite

of  $\text{PPh}_3$  to the reaction solution showed no change in rate or product distribution.

**Reversible Binding of  $\text{CO}_2$  to  $2^{\text{Ph}}$  and  $2^{\text{Cy}}$ .** Exposure of toluene solutions of  $2^{\text{Ph}}$  or  $2^{\text{Cy}}$  to  $\text{CO}_2$  at room temperature caused immediate precipitation of a voluminous white precipitate, in keeping with other reports on reaction of stannoxanes and carbon dioxide.<sup>18</sup> The use of methylene chloride as solvent led to production of clear solutions which could be studied by NMR and IR as described in the Supporting Information. Temperature dependent studies for  $2^{\text{Ph}}$  and  $2^{\text{Cy}}$  in methylene chloride solutions showed characteristic bands for the carbonate group<sup>19</sup> (see Figure S6 in the Supporting Information) for the band at  $1605\text{ cm}^{-1}$  assigned to one of two carbonate bands in the complex  $3^{\text{Cy}}$  as a function of  $\text{CO}_2$  pressure. There is an increase in intensity as the temperature is decreased which yielded equilibrium data. A plot of  $\ln(K_{\text{eq}})$  versus  $1/T$  yields  $\Delta H^\circ = -8.7 \pm 0.6\text{ kcal}\cdot\text{mol}^{-1}$ ,  $\Delta S^\circ = -17.1 \pm 2.0\text{ cal}\cdot\text{mol}^{-1}\cdot\text{K}^{-1}$ , and  $\Delta G^\circ_{298\text{K}} = -3.6 \pm 1.2\text{ kcal}\cdot\text{mol}^{-1}$  for the formation of  $3^{\text{Cy}}$  by reaction of  $2^{\text{Cy}}$  and  $\text{CO}_2$  (see Scheme 1) with all species in methylene chloride solution).

Attempts to determine thermodynamic data for the formation of  $3^{\text{Ph}}$ , which showed overall similar behavior to  $3^{\text{Cy}}$ , were frustrated due to the broadening of bands in the infrared spectrum which were temperature dependent. This was assigned to associative interactions in the less sterically encumbered  $3^{\text{Ph}}$  compared to  $3^{\text{Cy}}$ . This behavior appears to be common for stannoxane carbonates.<sup>18</sup>

**DFT Computational Studies of the Decomposition of *trans*-Bis-stannyl Hyponitrites.** DFT calculations were performed at the B3LYP-D3(BJ)/Def2-TZVP level of theory<sup>20–22</sup> in the gas phase to reveal the mechanism of the reactions observed experimentally (see Scheme 1). In this section, the elimination of nitrous oxide from *trans*- $[(\text{R}_3\text{Sn})_2(\mu\text{-N}_2\text{O}_2)]$  hyponitrite complexes is analyzed using the simpler *trans*- $[(\text{Me}_3\text{Sn})_2(\mu\text{-N}_2\text{O}_2)]$  hyponitrite  $1^{\text{Me}}$  in which the substituent groups of the tin atoms for the compounds experimentally studied,  $1^{\text{Ph}}$  ( $\text{R} = \text{Ph}$ ) and  $1^{\text{Cy}}$  ( $\text{R} = \text{Cy}$ ), have been replaced by methyl groups.

As stated in a previous section, in the crystalline structures of both  $1^{\text{Ph}}$  and  $1^{\text{Cy}}$ , the tin group is bent toward the  $\text{N}=\text{N}$  moiety, while that of the solid structure of  $[(\text{OEP})\text{Fe}]_2(\mu\text{-N}_2\text{O}_2)$ <sup>16</sup> is located away from it. Accordingly, the thermodynamic and kinetic parameters for the isomerization between both structures for the model  $1^{\text{Me}}$  compound ( $1^{\text{Me}}_{\text{a}}$  and  $1^{\text{Me}}_{\text{c}}$ ) were also computed, and the results are shown in Scheme 3.

As it can be seen in Scheme 3, the most thermodynamically stable isomer ( $1^{\text{Me}}_{\text{a}}$ ) exhibits the same configuration as that observed in the solid-state structure of  $1^{\text{Cy}}$  (see Figure 2) and  $1^{\text{Ph}}$ .<sup>13</sup> Nonetheless, the interconversion between all conformational isomers shown in Scheme 3 by rotation around the  $\text{N}-\text{O}$  bonds is facile as inferred by the activation enthalpies computed.

The computed Gibbs energy (and enthalpy) diagram for elimination of  $\text{N}_2\text{O}$  from  $1^{\text{Me}}$  is shown in Figure 7.

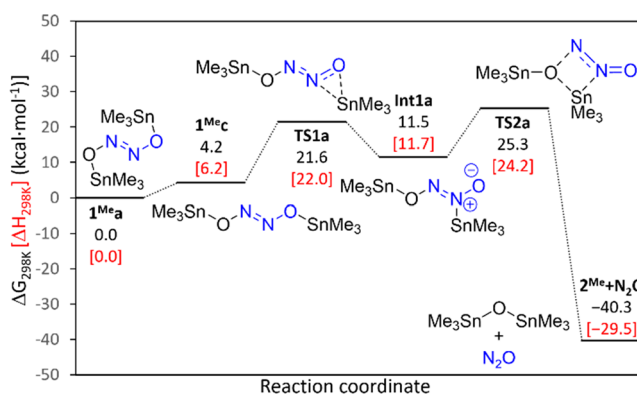


**Figure 7.** Schematic Gibbs energy and enthalpy diagram for elimination of  $\text{N}_2\text{O}$  from  $1^{\text{Me}}$  computed at the B3LYP<sup>20</sup>-D3(BJ)<sup>21</sup>/Def2-TZVP<sup>22</sup> level of theory (see the Supporting Information for further details). The isomerization steps for interconversion between  $1^{\text{Me}}_{\text{a}}$  and  $1^{\text{Me}}_{\text{c}}$  (Scheme 3) are not included in the figure.

An alternate mechanism with slightly higher barriers calculated for interconversion between  $1^{\text{Me}}_{\text{a}}$  and the key intermediate  $\text{Int1a}$  is shown in the Supporting Information. In Figure 7, the lowest energy TS leading to product goes through migration of the  $\text{Me}_3\text{Sn}$  group from the terminal O atom in the *trans* position through TS1, leading to the  $\text{Int1a}$  intermediate. A larger barrier exists for it to go forward to products than for it to go backward to starting material. The computed enthalpy of activation of extrusion of nitrous oxide from the most stable isomer of  $1^{\text{Me}}$  ( $1^{\text{Me}}_{\text{a}}$ ) of  $24.2\text{ kcal}\cdot\text{mol}^{-1}$  is in good agreement with the experimental value for  $1^{\text{Cy}}$  of  $22.7 \pm 2.5\text{ kcal}\cdot\text{mol}^{-1}$  at 298 K, while the activation entropy calculated for  $1^{\text{Me}}$  ( $-3.7\text{ cal}\cdot\text{mol}^{-1}\cdot\text{K}^{-1}$ ) is slightly less negative than that measured for  $1^{\text{Cy}}$  ( $-12.5 \pm 6\text{ cal}\cdot\text{mol}^{-1}\cdot\text{K}^{-1}$ ). However, the enthalpy of activation experimentally determined for  $\text{N}_2\text{O}$  elimination from  $1^{\text{Ph}}$  of  $15.8 \pm 2.0\text{ kcal}\cdot\text{mol}^{-1}$  is about  $7\text{ kcal}\cdot\text{mol}^{-1}$  lower and the entropy of activation is about  $16\text{ kcal}\cdot\text{mol}^{-1}$  less unfavorable (see Table 2). In this regard, calculations for the real complex  $1^{\text{Ph}}$  were also performed at the B3LYP-D3(BJ)/Def2-TZVP//B3LYP-D3(BJ)/Def2-SVP level of theory<sup>20–22</sup> in the gas phase in order to understand the discrepancy observed between the activation parameters experimentally measured and shown in Table 2 for  $1^{\text{Ph}}$  and  $1^{\text{Cy}}$ . The values computed,  $\Delta H^\ddagger$  ( $1^{\text{Ph}}$ ) =  $19.0\text{ kcal}\cdot\text{mol}^{-1}$  and  $\Delta S^\ddagger$  ( $1^{\text{Ph}}$ ) =  $-13.2\text{ cal}\cdot\text{mol}^{-1}\cdot\text{K}^{-1}$ , while higher than those experimentally determined, are  $6.3\text{ kcal}\cdot\text{mol}^{-1}$  and  $9.5\text{ cal}\cdot\text{mol}^{-1}\cdot\text{K}^{-1}$  lower than those previously calculated for the elimination of nitrous oxide from  $1^{\text{Me}}$  shown in Figure 7. Those differences are in line with the experimental activation parameters collected in Table 2 ( $\Delta\Delta H^\ddagger$  ( $1^{\text{Cy}}-1^{\text{Ph}}$ ) =  $6.9\text{ kcal}\cdot\text{mol}^{-1}$  and ( $\Delta\Delta S^\ddagger$  ( $1^{\text{Cy}}-1^{\text{Ph}}$ ) =

16 cal·mol<sup>-1</sup>·K<sup>-1</sup>) and are due to the establishment of stabilizing interactions between the phenyl groups linked to different tin atoms that are possible for the transition state but not for the **1<sup>Ph</sup>** hyponitrite since the two SnPh<sub>3</sub> moieties are far from each other. The optimized structure of the transition state (TS2<sup>Ph</sup>) for N<sub>2</sub>O elimination from **1<sup>Ph</sup>** is shown in Figure 8.

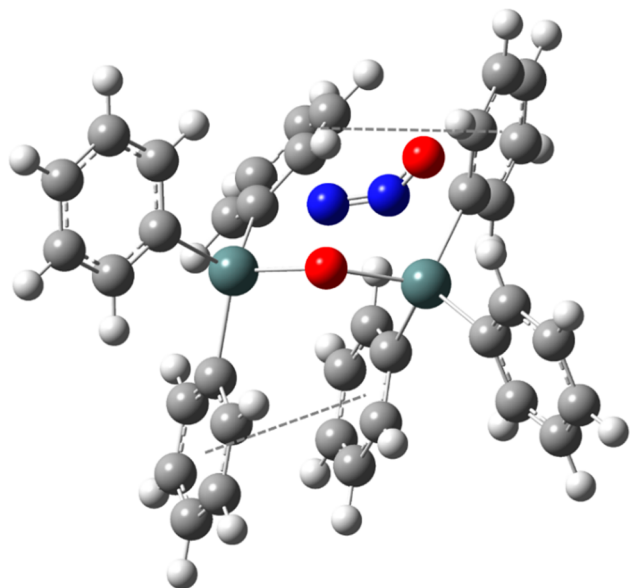


**Figure 8.** Optimized structure of the highest Gibbs energy transition state (TS2<sup>Ph</sup>) for N<sub>2</sub>O elimination from **1<sup>Ph</sup>** computed at the B3LYP-D3(BJ)/Def2-TZVP//B3LYP-D3(BJ)/Def2-SVP level of theory<sup>20–22</sup> in the gas phase. Selected intramolecular distances (in Å) and angles (in deg): O1–N1 = 1.775; N1–N2 = 1.199; N2–O2 = 1.254; Sn1–O1 = 2.062; Sn2–O1 = 2.102; Sn2–N2 = 2.836; Sn1–O–Sn2 = 129.7; Sn1–O1–N1 = 112.3; Sn2–O1–N1 = 109.4; O1–N1–N2 = 101.5; N1–N2–O2 = 133.2 [carbon (gray), nitrogen (blue), oxygen (red), tin (green), hydrogen (white)].

The  $\pi$ -stacking interactions that can be observed in the structure serve to stabilize the transition state and accordingly, to decrease the enthalpy of activation while the interactions make the structure less flexible, and consequently, a more unfavorable entropy of activation is obtained.

Finally, according to the principle of microscopic reversibility, the enthalpy and Gibbs energy of activation computed for N<sub>2</sub>O addition to Me<sub>3</sub>Sn–O–SnMe<sub>3</sub>, **2<sup>Me</sup>**, to yield the **1<sup>Me</sup>** hyponitrite (Figure 7) of 53.7 and 65.6 kcal·mol<sup>-1</sup>, respectively, are too high to occur at room temperature.

**Computational Study of Binding of CO<sub>2</sub> to **2<sup>Me</sup>**.** As discussed in the previous section, the carbon dioxide capture of bis-stannoxane compounds was also studied for the simpler Me<sub>3</sub>Sn–O–SnMe<sub>3</sub>, **2<sup>Me</sup>**, at the B3LYP-D3(BJ)/Def2-TZVP level of theory<sup>20–22</sup> in the gas phase. The binding and release of CO<sub>2</sub> are facile for both **2<sup>Cy</sup>** and **2<sup>Ph</sup>** as observed experimentally, and computed data for the simpler **2<sup>Me</sup>** model (Figure 9) are in agreement with that. The values in Figure 9 give insight into the process of initial CO<sub>2</sub> addition, followed by sequential rearrangement to the most stable **3<sup>Me</sup>** carbonate product. The computed value of  $\Delta H^\circ = -9.3$  kcal·mol<sup>-1</sup> shown in Figure 9 for CO<sub>2</sub> capture by **2<sup>Me</sup>** is in excellent agreement with that determined experimentally for CO<sub>2</sub> addition to **2<sup>Cy</sup>** of  $\Delta H^\circ = -8.7 \pm 0.6$  kcal·mol<sup>-1</sup>.

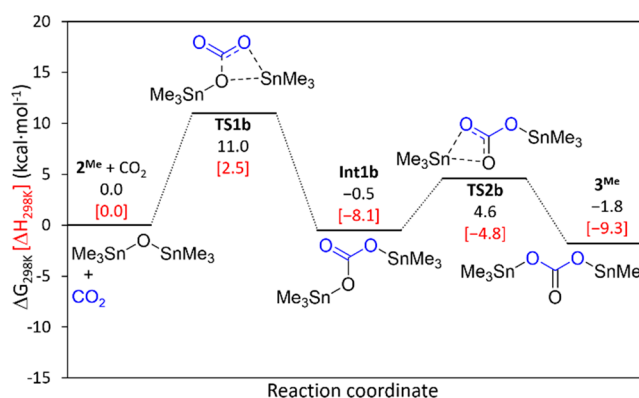
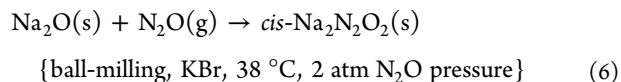


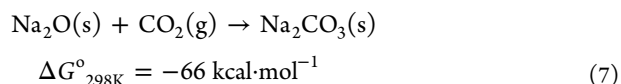
**Figure 9.** Schematic Gibbs energy and enthalpy diagram for addition of CO<sub>2</sub> to **2<sup>Me</sup>** and subsequent isomerization to the final product **3<sup>Me</sup>** computed at the B3LYP<sup>20</sup>-D3(BJ)<sup>21</sup>/Def2-TZVP<sup>22</sup> level of theory.

## DISCUSSION

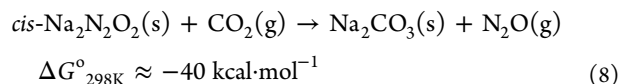
Metal complexes of hyponitrites are much less common than the ubiquitous carbonate analogues. For example, we have recently reported<sup>5</sup> generation of *cis*-Na<sub>2</sub>N<sub>2</sub>O<sub>2</sub> by the ball-milling reaction shown in reaction 6.



The only prior report of direct reaction was that of Feldmann and Jansen at 360 °C in a tube furnace preparation. These observations indicate net favorable thermodynamics for the insertion process of N<sub>2</sub>O. The analogous reaction to form sodium carbonate is also thermodynamically favorable as shown in eq 7.<sup>23</sup>

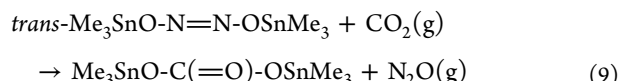


Reaction 6 is one of the few reported reactions in which nitrous oxide inserts into a metal oxide directly. Computational studies<sup>24</sup> yield a value of  $\Delta G^\circ_{298\text{K}} \approx -26$  kcal·mol<sup>-1</sup> for eq 6. Subtracting eq 6 from eq 7 yields eq 8 for which the Gibbs energy change can be estimated using the thermodynamic value for reaction 7 and that computed for reaction 6 and as shown in eq 8.



The current work reports studies of binding of N<sub>2</sub>O and CO<sub>2</sub> at R<sub>3</sub>Sn–O–SnR<sub>3</sub>. This will allow comparison of the main group metal Sn to the alkali metal Na. Work in progress is aimed at kinetic and thermodynamic studies of Pt containing hyponitrites and carbonates. It is hoped that trends may emerge suggesting how best to approach new reaction chemistry of nitrous oxide. Considerable work in this area has been reported by Severin<sup>25</sup> and Hayton.<sup>26</sup>

The Gibbs energy value estimated for displacement of N<sub>2</sub>O by CO<sub>2</sub> from *cis*-Na<sub>2</sub>N<sub>2</sub>O<sub>2</sub> as shown in eq 8 may be compared to the computed value for the analogous reaction for the tin hyponitrite **1<sup>Me</sup>** studied in this work as shown in eq 9.



The calculated Gibbs energy change for addition of  $\text{N}_2\text{O}$  to  $\text{Me}_3\text{Sn-O-SnMe}_3$  ( $2^{\text{Me}}$ ) is  $\Delta G_{298\text{K}}^\circ = +40.3 \text{ kcal}\cdot\text{mol}^{-1}$  as it can be seen in Figure 7. The computed  $\Delta G_{298\text{K}}^\circ$  value for  $\text{CO}_2$  insertion into the Sn–O bond of  $2^{\text{Me}}$  to make the monomeric carbonate complex,  $3^{\text{Me}}$ , as shown in Figure 9, is  $\Delta G_{298\text{K}}^\circ = -1.8 \text{ kcal}\cdot\text{mol}^{-1}$ . Confidence in that value is gained by the derived experimental value from the graph in SI Figure S6 of  $\Delta G_{298\text{K}}^\circ = -3.6 \pm 1.2 \text{ kcal}\cdot\text{mol}^{-1}$  for the analogous reaction with  $3^{\text{Cy}}$ . Utilizing these data yields an estimate of  $\Delta G_{298\text{K}}^\circ = -44 \text{ kcal}\cdot\text{mol}^{-1}$  for displacement of bound  $\text{N}_2\text{O}$  by  $\text{CO}_2$  in reaction 9. This is surprisingly close to the estimate made for reaction 8 of  $\Delta G_{298\text{K}}^\circ = -40 \text{ kcal}\cdot\text{mol}^{-1}$ . The relatively close agreement assigned to conversion of a hyponitrite to a carbonate for  $\text{Na}_2\text{O}$  and  $\text{Me}_3\text{SnOSnMe}_3$  appears to imply that the dominant factor determining the relative stability may lie in the hypothetical  $\text{O}^{2-}$  transfer reaction shown in reaction 10 and relative Lux acidity<sup>27</sup> of  $\text{N}_2\text{O}$  and  $\text{CO}_2$ , and that this is closely related to resonance delocalization and charge stabilization in the carbonate ion being greater than that of the hyponitrite ion.



The Gibbs energy at 298 K for the acid base reaction shown in reaction 10 is computed to be  $-48.1$  and  $-46.0 \text{ kcal}\cdot\text{mol}^{-1}$  for the *cis*- and *trans*- $\text{N}_2\text{O}_2^{2-}$  anions, respectively, at the B3LYP-D3(BJ)/Def2-TZVP level of theory.<sup>20–22</sup> These values are only slightly higher than those computed for reactions 8 and 9, supporting the hypothesis that the most relevant energetic contribution to these reactions is related to the difference in resonance delocalization and charge stabilization in the ions and simple binding reactions of  $\text{CO}_2$  and  $\text{N}_2\text{O}$  to  $\text{Na}_2\text{O}$  or *trans*- $\text{Me}_3\text{SnOSnMe}_3$ , as discussed earlier, may be similar in reaction energy. Additional experimental work to further support that hypothesis is planned.

In benzene solution in sealed NMR tube studies, the first order decay of the hyponitrite complexes and their impervious response to added  $\text{PPh}_3$ ,  $\text{O}_2$ ,  $\text{CO}_2$ , and  $\text{N}_2\text{O}$  were surprising. This is in keeping with the computed mechanism that involves migration of the Sn group from O to N as shown in Figure 7. It is of interest to compare the mechanism computed in this work for  $\text{N}_2\text{O}$  elimination from the hyponitrite  $1^{\text{Me}}$  to the well studied mechanism for dissociation of *trans*- $\text{H}_2\text{N}_2\text{O}_2$  hyponitrous acid computed previously by Morokuma<sup>28</sup> and more recently by Thynell.<sup>29</sup> Figure 10 shows a comparison of the mechanism for the reverse reaction:  $\text{N}_2\text{O}$  addition to  $\text{H}_2\text{O}$  (previously computed)<sup>30</sup> or to  $\text{Me}_3\text{SnOSnMe}_3$  (computed in this work, see Figure 7) to yield *trans*- $\text{H}_2\text{N}_2\text{O}_2$  or hyponitrite  $1^{\text{Me}}$ , respectively.

$\text{N}_2\text{O}$  capture processes by either water or  $\text{Me}_3\text{SnOSnMe}_3$  to form *trans*-hyponitrous acid or the *trans*-hyponitrite  $1^{\text{Me}}$  complex are both highly endergonic processes ( $\Delta G_{298\text{K}}^\circ \approx +53$  and  $+40 \text{ kcal}\cdot\text{mol}^{-1}$ , respectively). The transition states and intermediates for both tin and hyponitrous acid are very similar with no readily discernible difference. The Gibbs energy barrier however is substantially higher for water than it is for tin ( $+120$  vs  $+65 \text{ kcal}\cdot\text{mol}^{-1}$ ). The ability of tin to become hypervalent is the most probable reason for this. In either TS, tin is able to obtain substantial donation from both the N and the O lone pairs while migrating due to its larger

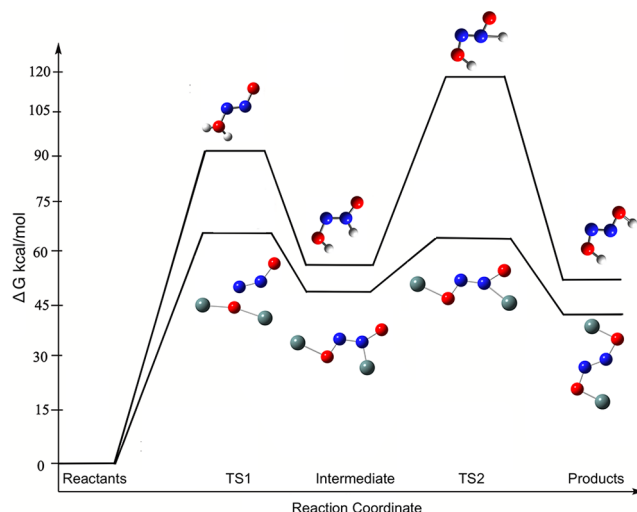


**Figure 10.** Reaction profile ( $\text{kcal}\cdot\text{mol}^{-1}$ ) for the unfavorable addition of  $\text{N}_2\text{O}$  to  $\text{H}_2\text{O}$  and  $\text{Me}_3\text{SnOSnMe}_3$ . Data for reaction of  $\text{H}_2\text{O}$  and  $\text{N}_2\text{O}$  leading to *trans*- $\text{H}_2\text{N}_2\text{O}_2$  are from Thynell<sup>29</sup> [carbon (gray), nitrogen (blue), oxygen (red), tin (green), hydrogen (white)].

size and vacant  $5d$  orbitals. In contrast, H migration requires substantial weakening of the O–H bond, contributing to its higher activation energy.

The rapid reaction of protic acids to eliminate  $\text{H}_2\text{N}_2\text{O}_2$  which subsequently decomposes to  $\text{H}_2\text{O}$  and  $\text{N}_2\text{O}$  in an acid catalyzed reaction is a characteristic reaction of hyponitrites.<sup>1,2</sup> Reaction of  $1^{\text{Ph}}$  or  $1^{\text{Cy}}$  with the transition metal carbonyl hydride  $\text{H-Cr}(\text{CO})_3\text{C}_5\text{Me}_5$  is rapid and produces  $\text{Ph}_3\text{Sn-Cr}(\text{CO})_3\text{C}_5\text{Me}_5$  and  $\text{H}_2\text{N}_2\text{O}_2$  in high yields in organic solvents. Since tin hyponitrites are stable, anhydrous, and store well under dry argon, combined with the fact that the chromium hydride may be prepared in high purity and that  $\text{R}_3\text{Sn-Cr}(\text{CO})_3\text{C}_5\text{Me}_5$ , **CrSn**, products are nonvolatile, the reaction of tin hyponitrites with  $\text{H-Cr}(\text{CO})_3\text{C}_5\text{Me}_5$  presents a convenient method to prepare and vacuum transfer anhydrous hyponitrous acid which may be of synthetic utility.

It is well-known that organic hyponitrites are decomposed by radicals and either alkyl or alkoxy radicals may be produced during this process. The tin hyponitrites, since they are large and also contain vacant  $5d$  orbitals, are a ready radical receptor, and radical addition at the Sn center to form a hypervalent tin radical intermediate appears to be more facile for stannyl as opposed to alkyl hyponitrites. Investigation of reactions of the 17 electron organometallic radical  $\bullet\text{Cr}(\text{CO})_3\text{C}_5\text{Me}_5$  and  $1^{\text{Ph}}$  shows concentration dependent behavior, and a plethora of products are formed. These complex reactions are under additional mechanistic investigation, but several observations may be made at this time. At low radical concentrations, where concerted attack of two  $\bullet\text{Cr}(\text{CO})_3\text{C}_5\text{Me}_5$  radicals is disfavored, elimination of  $\text{N}_2\text{O}$  from the tin hyponitrites is moderately accelerated as proposed via generation of the  $\text{Ph}_3\text{SnO}\bullet$  radical which serves as a radical carrier for nitrous oxide elimination as shown in Scheme 2.

At higher  $\text{Cr}\bullet$  concentrations, a more complex behavior was observed. Carbon dioxide was evolved, and in addition, an unstable intermediate complex as  $\text{Cr}(\text{Cp}^*)(\text{CO})_2(\text{NNO-SnPh}_3)$  is formed together with detectable  $\text{CO}_2$  evolution. When reactions of  $1^{\text{Ph}}$  are done with  $\text{H-Cr}(\text{CO})_3\text{C}_5\text{Me}_5$  (which like  $\text{H-Cr}(\text{CO})_3\text{C}_5\text{H}_5$  is both a weak acid and a facile H atom transfer reagent), there is a more rapid evolution of

N<sub>2</sub>O and near quantitative formation of Ph<sub>3</sub>Sn-Cr-(CO)<sub>3</sub>C<sub>5</sub>Me<sub>5</sub> and H<sub>2</sub>O. While this resembles reactions of other protic acids, the role of radical and H atom transfer reactions can not be ruled out.

## CONCLUSIONS

Experimental studies of the rate of loss of N<sub>2</sub>O from **1**<sup>Ph</sup> and **1**<sup>Cy</sup> are in good agreement with computational studies for **1**<sup>Me</sup>. The reaction is impervious to added N<sub>2</sub>O, CO<sub>2</sub>, O<sub>2</sub>, and PPh<sub>3</sub>, which is in keeping with the concerted migration pathway computed for **1**<sup>Me</sup> and also closely resembles published work for H<sub>2</sub>N<sub>2</sub>O<sub>2</sub>(g)<sup>29</sup> with larger computed barriers found for hyponitrous acid than for **1**<sup>Me</sup>. The lower activation energy for loss of nitrous oxide from the tin hyponitrites compared to hyponitrous acid is attributed to more facile mobility of the tin group compared to the proton. The computed estimate for ΔG<sup>o</sup><sub>298K</sub> for displacement of N<sub>2</sub>O from a hyponitrite by CO<sub>2</sub> to form a carbonate was found to be similar for **1**<sup>Me</sup> (−44 kcal·mol<sup>−1</sup>) and *cis*-Na<sub>2</sub>N<sub>2</sub>O<sub>2</sub> (−40 kcal·mol<sup>−1</sup>). This may imply that, while the absolute value of hyponitrite binding may vary considerably, the relative stability of hyponitrite and carbonate binding may be similar. Additional experimental and computational work is in progress<sup>30</sup> with sodium oxide and other metal oxides with high Lux basicity<sup>27</sup> to further map kinetic and thermodynamic factors controlling the reactivity of hyponitrites.

## ASSOCIATED CONTENT

### Supporting Information

The Supporting Information is available free of charge at <https://pubs.acs.org/doi/10.1021/acs.inorgchem.1c01291>.

Additional experimental data, synthetic procedures, characterization of compounds, and DFT calculations (PDF)

### Accession Codes

CCDC 2079922 contains the supplementary crystallographic data for this paper. These data can be obtained free of charge via [www.ccdc.cam.ac.uk/data\\_request/cif](http://www.ccdc.cam.ac.uk/data_request/cif), or by emailing [data\\_request@ccdc.cam.ac.uk](mailto:data_request@ccdc.cam.ac.uk), or by contacting The Cambridge Crystallographic Data Centre, 12 Union Road, Cambridge CB2 1EZ, UK; fax: +44 1223 336033.

## AUTHOR INFORMATION

### Corresponding Authors

**Burjor Captain** – Department of Chemistry, University of Miami, Coral Gables, Florida 33146, United States; [orcid.org/0000-0002-7272-5655](https://orcid.org/0000-0002-7272-5655); Email: [captain@miami.edu](mailto:captain@miami.edu)

**Manuel Temprado** – Departamento de Química Analítica, Química Física e Ingeniería Química, Instituto de Investigación Química “Andrés M. del Río”, Universidad de Alcalá, 28871 Madrid, Spain; [orcid.org/0000-0002-2003-4588](https://orcid.org/0000-0002-2003-4588); Email: [manuel.temprado@uah.es](mailto:manuel.temprado@uah.es)

**Carl D. Hoff** – Department of Chemistry, University of Miami, Coral Gables, Florida 33146, United States; [orcid.org/0000-0002-0100-7293](https://orcid.org/0000-0002-0100-7293); Email: [c.hoff@miami.edu](mailto:c.hoff@miami.edu)

### Authors

**Jack V. Davis** – Department of Chemistry, University of Miami, Coral Gables, Florida 33146, United States

**Mohan M. Gamage** – Department of Chemistry, University of Miami, Coral Gables, Florida 33146, United States

**Oswaldo Guio** – Department of Chemistry, University of Miami, Coral Gables, Florida 33146, United States

Complete contact information is available at: <https://pubs.acs.org/10.1021/acs.inorgchem.1c01291>

### Author Contributions

<sup>§</sup>Equally contributing authors.

### Author Contributions

All authors have given approval to the final version of the manuscript.

### Funding

The Department of Energy DOE-BES-DE-SC0019456 and the Ministerio de Economía y Competitividad, Spain (CTQ2016-80600-P) are gratefully acknowledged for support of this work.

### Notes

The authors declare no competing financial interest.

## REFERENCES

- (1) Van Stappen, C.; Lehnert, N. Mechanism of N–N Bond Formation by Transition Metal–Nitrosyl Complexes: Modeling Flavodiiron Nitric Oxide Reductases. *Inorg. Chem.* **2018**, *57*, 4252–4269.
- (2) (a) Hughes, M. N.; Stedman, G. 231. Kinetics and mechanism of the decomposition of hyponitrous acid. *J. Chem. Soc.* **1963**, 1239–1243. (b) Buchholz, J. R.; Powell, R. E. The Decomposition of Hyponitrous Acid. I. The Non-chain Reaction. *J. Am. Chem. Soc.* **1963**, *85*, 509–511. (c) Buchholz, J. R.; Powell, R. E. The Decomposition of Hyponitrous Acid. II. The Chain Reaction. *J. Am. Chem. Soc.* **1965**, *87*, 2350–2353. (d) Poskrebyshv, G. A.; Shafirovich, V.; Lyman, S. V. Hyponitrite Radical, a Stable Adduct of Nitric Oxide and Nitroxyl. *J. Am. Chem. Soc.* **2004**, *126*, 891–899.
- (3) (a) Mendenhall, G. D.; Stewart, L. C.; Scaiano, J. C. Laser photolysis study of the reactions of alkoxy radicals generated in the photosensitized decomposition of organic hyponitrites. *J. Am. Chem. Soc.* **1982**, *104*, 5109–5114. (b) Ogle, C. A.; Martin, S. W.; Dziobak, M. P.; Urban, M. W.; Mendenhall, G. D. Decomposition Rates, Synthesis, and Spectral Properties of a Series of Alkyl Hyponitrites. *J. Org. Chem.* **1983**, *48*, 3728–3733.
- (4) (a) Feldmann, C.; Jansen, M. Zur Kenntnis von *cis*-Natrium hyponitrit. *Z. Anorg. Allg. Chem.* **1997**, *623*, 1803–1809. (b) Feldmann, C.; Jansen, M. *cis*-Sodium hyponitrite - A new route and a crystal structure analysis. *Angew. Chem., Int. Ed. Engl.* **1996**, *35*, 1728–1730.
- (5) Davis, J. V.; Guio, O.; Captain, B.; Hoff, C. D. Production of *cis*-Na<sub>2</sub>N<sub>2</sub>O<sub>2</sub> and NaNO<sub>3</sub> by ball milling Na<sub>2</sub>O and N<sub>2</sub>O in alkali metal halide salts. *ACS Omega* **2021**, *6*, 18248–18252.
- (6) Sumida, K.; Rogow, D. L.; Mason, J. A.; McDonald, T. M.; Bloch, E. D.; Herm, Z. R.; Bae, T. H.; Long, J. R. Carbon Dioxide Capture in Metal–Organic Frameworks. *Chem. Rev.* **2012**, *112*, 724–781.
- (7) Duong, H. A.; Tekavec, T. N.; Arif, A. M.; Louie, J. Reversible carboxylation of N-heterocyclic carbenes. *Chem. Commun.* **2004**, 112–113.
- (8) Tskhovrebov, A. G.; Solari, E.; Wodrich, M. D.; Scopelliti, R.; Severin, K. Covalent Capture of Nitrous Oxide by N-Heterocyclic Carbenes. *Angew. Chem., Int. Ed.* **2012**, *51*, 232–234.
- (9) Arduengo, A. J.; Krafczyk, R.; Schmutzler, R.; Craig, H. A.; Goerlich, J. R.; Marshall, W. J.; Unverzagt, M. Imidazolylidenes, imidazolylidenes and imidazolidines. *Tetrahedron* **1999**, *55*, 14523–14534.
- (10) Temprado, M.; Majumdar, S.; Cai, X.; Captain, B.; Hoff, C. D. Synthesis, structure, and thermochemistry of adduct formation between N-heterocyclic carbenes and isocyanates or mesitylnitrite oxide. *Struct. Chem.* **2013**, *24*, 2059–2068.
- (11) Lombardi, B. M. P.; Gendy, C.; Gelfand, B. S.; Bernard, G. M.; Wasylshen, R. E.; Tuononen, H. M.; Roesler, R. Side-on

Coordination in Isostructural Nitrous Oxide and Carbon Dioxide Complexes of Nickel. *Angew. Chem., Int. Ed.* **2021**, *60*, 7077–7081.

(12) Beck, W.; Engelmann, H.; Smedal, H. S. Bis(triphenylzinn-und-blei)hyponitrit  $[(C_6H_5)_3M]_2N_2O_2$  (M = Sn, Pb). *Z. Anorg. Allg. Chem.* **1968**, *357*, 134–138.

(13) Mayer, T.; Beck, W.; Böttcher, H.-C. Crystal and Molecular Structure of the trans- Hyponitrite Compound  $Ph_3Sn(\mu\text{-ONNO})\text{-}SnPh_3$ . *Z. Anorg. Allg. Chem.* **2011**, *637*, 345–347.

(14) Sato, H. A Bridge-type Sn...O Coordination of Bis(trialkyltin) Carbonates. *Bull. Chem. Soc. Jpn.* **1967**, *40*, 410–410.

(15) (a) Ma, C.; Tian, G.; Zhang, R. New triorganotin(IV) complexes of polyfunctional S,N,O-ligands: Supramolecular structures based on  $\pi\cdots\pi$  and/or C–H... $\pi$  interactions. *J. Organomet. Chem.* **2006**, *691*, 2014–2022. (b) Wakamatsu, K.; Orita, A.; Otera, J. DFT Study on Activation of Carbon Dioxide by Dimethyltin Dimethoxide for Synthesis of Dimethyl Carbonate. *Organometallics* **2010**, *29*, 1290–1295.

(16) Berto, T. C.; Xu, N.; Lee, S. R.; McNeil, A. J.; Alp, E. E.; Zhao, J.; Richter-Addo, G. B.; Lehnert, N. Characterization of the Bridged Hyponitrite Complex  $\{[Fe(OEP)]_2(\mu\text{-}N_2O_2)\}$ : Reactivity of Hyponitrite Complexes and Biological Relevance. *Inorg. Chem.* **2014**, *53*, 6398–6414.

(17) (a) Cai, X.; Majumdar, S.; Fortman, G. C.; Koppaka, A.; Serafim, L.; Captain, B.; Temprado, M.; Hoff, C. D. Thermodynamic, Kinetic, Structural, and Computational Studies of the  $Ph_3Sn\text{-}H, Ph_3Sn\text{-}SnPh_3$ , and  $Ph_3Sn\text{-}Cr(CO)_3C_5Me_5$  Bond Dissociation Enthalpies. *Inorg. Chem.* **2016**, *55*, 10751–10766. (b) Capps, K. B.; Bauer, A.; Sukcharoenphon, K.; Hoff, C. D. Kinetic and Thermodynamic Studies of Reaction of  $\bullet Cr(CO)_3C_5Me_5$ ,  $HCr(CO)_3C_5Me_5$ , and  $PhSCr(CO)_3C_5Me_5$  with  $\bullet NO$ . Reductive Elimination of Thermodynamically Unstable Molecules HNO and RSNO Driven by Formation of the Strong Cr–NO Bond. *Inorg. Chem.* **1999**, *38*, 6206–6211.

(18) Plasseraud, L.  $CO_2$  Derivatives of Molecular Tin Compounds. Part 1: Hemicarbonato and Carbonato Complexes. *Inorganics* **2020**, *8*, 31.

(19) Nakamoto, K. *Infrared and Raman Spectra of Inorganic and Coordination Compounds, Part A: Theory and Applications in Inorganic Chemistry*, 6th ed.; Wiley: New York, 2009.

(20) (a) Becke, A. D. Density-functional thermochemistry. III. The role of exact exchange. *J. Chem. Phys.* **1993**, *98*, 5648–5652. (b) Lee, C.; Yang, W.; Parr, R. G. Development of the Colle-Salvetti correlation-energy formula into a functional of the electron density. *Phys. Rev. B: Condens. Matter Mater. Phys.* **1988**, *37*, 785–789.

(21) Grimme, S.; Ehrlich, S.; Goerigk, L. Effect of the damping function in dispersion corrected density functional theory. *J. Comput. Chem.* **2011**, *32*, 1456–1465.

(22) Weigend, F.; Ahlrichs, R. Balanced basis sets of split valence, triple zeta valence and quadruple zeta valence quality for H to Rn: Design and assessment of accuracy. *Phys. Chem. Chem. Phys.* **2005**, *7*, 3297–3305.

(23) Thermochemical data are derived from <https://webbook.nist.gov/chemistry/> and related online sources.

(24) Temprado, M.; Davis, J. V.; Guio, O.; Hoff, C. D. Unpublished results.

(25) Severin, K. Synthetic chemistry with nitrous oxide. *Chem. Soc. Rev.* **2015**, *44*, 6375–6386.

(26) Wright, A. M.; Hayton, T. W. Understanding the Role of Hyponitrite in Nitric Oxide Reduction. *Inorg. Chem.* **2015**, *54*, 9330–9341.

(27) Weller, J. M.; Chan, C. K. Reduction in Formation Temperature of Ta-Doped Lithium Lanthanum Zirconate by Application of Lux-Flood Basic Molten Salt Synthesis. *ACS Appl. Energy Mater.* **2020**, *3*, 6466–6475.

(28) Mebel, A. M.; Morokuma, K.; Lin, M. C.; Melius, C. F. Potential Energy Surface of the HNO + NO Reaction. An ab Initio Molecular Orbital Study. *J. Phys. Chem.* **1995**, *99*, 1900–1908.

(29) Zhang, K.; Thynell, S. T. Examination of the Mechanism of the Yield of  $N_2O$  from Nitroxyl (HNO) in the Solution Phase by Theoretical Calculations. *J. Phys. Chem. A* **2017**, *121*, 4505–4516.

(30) Davis, J. V.; Guio, O.; Gamage, M. M.; Captain, B.; Temprado, M.; Hoff, C. D., work in progress.